International Journal of Mass Spectrometry 291 (2010) 84–89

Contents lists available at ScienceDirect

International Journal of Mass Spectrometry

journal homepage: www.elsevier.com/locate/ijms

Diastereoselective gas-phase ion/molecule reactions of ethanolamine neurotransmitter/amido[4]resorcinarene adducts

Maurizio Speranza[a,*], Ilaria D'Acquarica[a], Caterina Fraschetti[a], Bruno Botta[a], Andrea Tafi[b], Luca Bellucci[b], Giovanni Zappia[c]

[a] Dipartimento di Chimica e Tecnologie del Farmaco, Sapienza-Università di Roma, Piazzale Aldo Moro 5, I-00185 Roma, Italy
[b] Dipartimento Farmaco Chimico Tecnologico, Università di Siena, 53100 Siena, Italy
[c] Istituto di Chimica Farmaceutica, Università degli Studi di Urbino "Carlo Bo", 61029 Urbino, Italy

ARTICLE INFO

Article history:
Received 9 November 2009
Received in revised form
10 December 2009
Accepted 22 January 2010
Available online 1 February 2010

Keywords:
Diastereoselectivity
Host/guest complexes
Kinetics
FT-ICR mass spectrometry
Molecular dynamics

ABSTRACT

Fourier-Transform Ion Cyclotron Resonance (FT-ICR) kinetic experiments, supported by molecular mechanics calculations and molecular dynamics simulations, indicate that the relative stability of the diastereomeric proton-bound adducts between some ethanolamine neurotransmitters and a chiral amido[4]resorcinarene receptor depends on the relative position and orientation of the hydroxyl and amino functionalities on the neurotransmitter side chain, on the presence of the methyl substituent on its N center, as well as on the specific group of the receptor proton-bonded to the amino group of the ethanolamine. These factors strongly influence the nature and the intensity of the noncovalent interactions in the ethanolamine/amido[4]resorcinarene adducts and, therefore, their reactivity towards 2-aminobutane enantiomers.

1. Introduction

In a recent study, some information was provided on the nature of the specific noncovalent interactions in several proton-bound adducts between the amphetamine enantiomers $\mathbf{1^S}$ and $\mathbf{1^R}$ and several receptor mimics, including the chiral amido[4]resorcinarene $\mathbf{M^S}$ (Fig. 1) [1]. Interest in proton-bonded host/guest systems arises from the fact that basic amines, like amphetamine, may exist in the protonated form under physiological conditions [2]. Furthermore, the study was carried out in the gas phase, namely under conditions mimicking the extensive desolvation of N-protonated amphetamine when interacting with the receptor pocket [3]. The experimental results, supported by computational evidence, indicated that the gas-phase stability of the diastereomeric $[\mathbf{M^S}{\cdot}\mathrm{H}{\cdot}\mathbf{A}]^+$ ($\mathbf{A} = \mathbf{1^S}$; $\mathbf{1^R}$) adducts and their reactivity towards the enantiomers of 2-aminobutane ($\mathbf{B^R}$ and $\mathbf{B^S}$; Eq. (1)) depend on structural and dynamic factors, including the oscillation frequency and amplitude of the guest **A** placed outside the chiral cavity of the protonated host chiral cavity (the *ext* position in Fig. 1).

$$[\mathbf{M^S}{\cdot}\mathrm{H}{\cdot}\mathbf{A}]^+ + \mathbf{B} \rightarrow [\mathbf{M^S}{\cdot}\mathrm{H}{\cdot}\mathbf{B}]^+ + \mathbf{A} \quad (1)$$

The study is now extended to some important members of the ethanolamine neurotransmitters family, i.e., the enantiomers of phenylalaninol ($\mathbf{2^{R/S}}$), ephedrine ($\mathbf{3^{RS/SR}}$), and pseudoephedrine ($\mathbf{4^{RR/SS}}$) (Fig. 2), with the aim of verifying whether and to what extent the presence of the OH functionality and its orientation in the molecule influence the relative stability of the relevant $[\mathbf{M^S}{\cdot}\mathrm{H}{\cdot}\mathbf{A}]^+$ adducts and the efficiency and selectivity of their reaction with the enantiomers of 2-aminobutane (Eq. (1)).

2. Experimental

2.1. Materials

Enantiomerically pure $\mathbf{M^S}$, in the flattened-cone conformation, was synthesized and purified according to the established procedures [4]. The pure D- and L-enantiomers of the hydrochlorides of the neurotransmitters **A** ($\mathbf{A}H^+{\cdot}Cl^-$; **A** = ephedrine ($\mathbf{3^{RS/SR}}$); pseudoephedrine ($\mathbf{4^{RR/SS}}$)) were purchased from a commercial source and used without further purification. The same source provided the (*R*)-(−)-($\mathbf{B^R}$) and (*S*)-(+)-2-aminobutane ($\mathbf{B^S}$), which were purified in the vacuum manifold with several freeze–thaw cycles. The pure enantiomers of phenylalaninol ($\mathbf{2^{R/S}}$) were synthe-

* Corresponding author. Tel.: +39 06 4991 3497; fax: +39 06 4991 3497.
E-mail address: maurizio.speranza@uniroma1.it (M. Speranza).

1387-3806/$ – see front matter © 2010 Elsevier B.V. All rights reserved.
doi:10.1016/j.ijms.2010.01.017

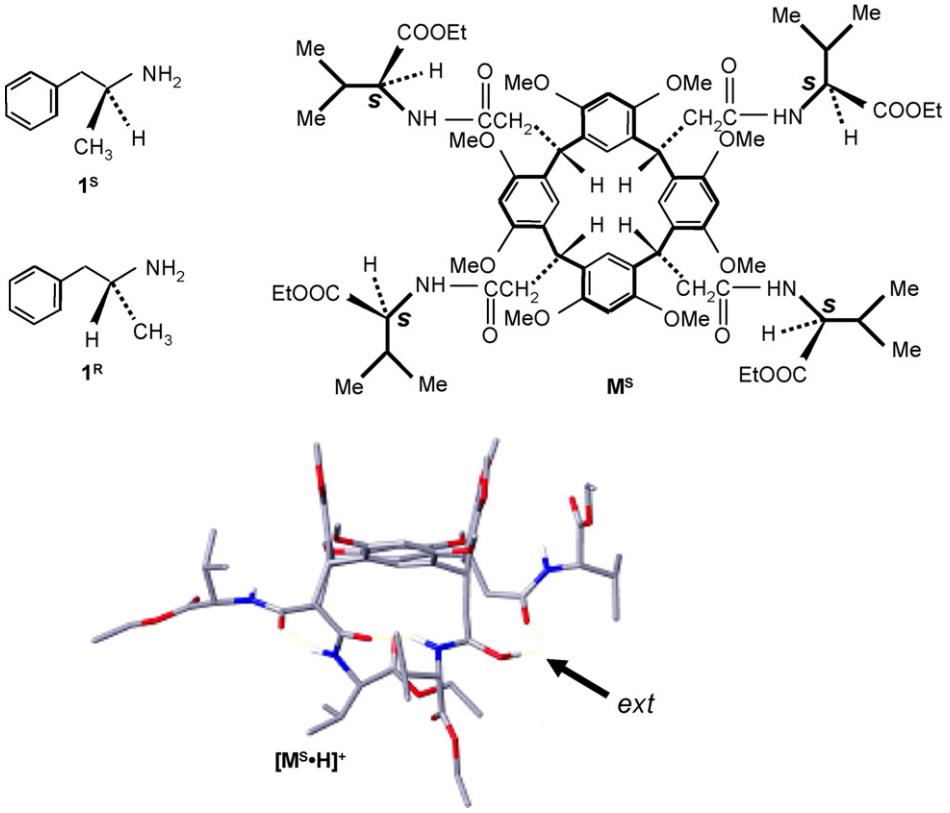

Fig. 1. Formulas and symbols of the amphetamine enantiomers $\mathbf{1^S}$ and $\mathbf{1^R}$ and of the flattened-cone 2,8,14,20-tetrakis(L-valinamido)resorcin[4]arene ethyl tetra-ester ($\mathbf{M^S}$). The preferred external position of amphetamine in $[\mathbf{M^S}{\cdot}H{\cdot}\mathbf{1^S}]^+$ and $[\mathbf{M^S}{\cdot}H{\cdot}\mathbf{1^R}]^+$ from MD simulations (Ref. [1]).

sized (e.e. > 99%) by $LiBH_4$/TMSCl reduction from the corresponding amino acids according to Quagliato et al. [5]. The free neurotransmitters **A** were obtained by treating the corresponding hydrochlorides with 1N $NaHCO_3$ water solutions.

2.2. FT-ICR experiments

The experiments were carried out as described elsewhere [1]. In particular, they were performed at room temperature in an APEX 47e FT-ICR mass spectrometer equipped with an ESI source (Bruker Spectrospin) and a resonance cell ("infinity cell") situated between the poles of a superconducting magnet (4.7 T). Stock CH_3OH solutions of $\mathbf{M^S}$ (1×10^{-5} M), containing a fivefold excess of the appropriate **A** enantiomer were electrosprayed through a heated capillary (130 °C) into the external source of the FT-ICR mass spectrometer. The resulting ions were transferred into the resonance cell by a system of potentials and lenses and quenched by collisions with methane pulsed into the cell through a magnetic valve. ESI of $\mathbf{M^S}$/**A** methanolic solutions leads to the formation of abundant signals, corresponding to the natural isotopomers of the proton-bound adduct $[\mathbf{M^S}{\cdot}H{\cdot}\mathbf{A}]^+$. Once isolated by broad-band ejection from the accompanying ions, the $[\mathbf{M^S}{\cdot}H{\cdot}\mathbf{A}]^+$ adduct was allowed to react with the 2-aminobutane **B** enantiomers present in the cell at a fixed pressure whose value ranges from 4.6×10^{-8} to 1.1×10^{-7} mbar depending upon the reactivity of the specific adducts.

Collision induced decompositon (CID) experiments on the $[\mathbf{M^S}{\cdot}H{\cdot}\mathbf{A}]^+$ adducts lead to the exclusive formation of the $[\mathbf{M^S}{\cdot}H]^+$ fragment, irrespective of the collision energy (E_{lab} = 10–30 eV), thus suggesting that the proton in $[\mathbf{M^S}{\cdot}H{\cdot}\mathbf{A}]^+$ is preferentially located on one of the amidocarbonyl moieties of $\mathbf{M^S}$, rather than on the amino group of **A**.

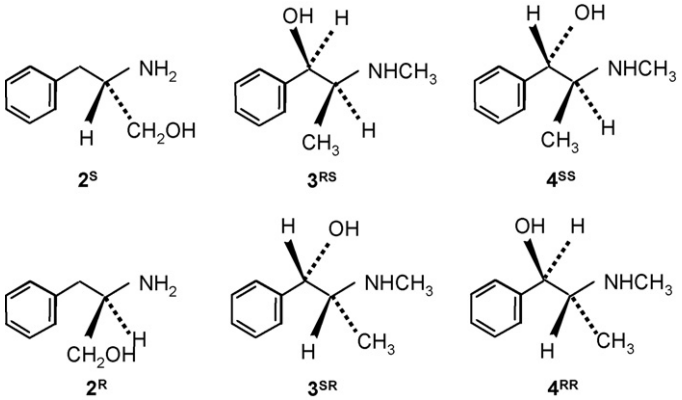

Fig. 2. Formulas and symbols of the selected ethanolamine neurotransmitters.

2.3. Docking and molecular dynamics calculations

All the computational calculations were carried out and visualized on Intel Linux PCs incorporating Pentium IV CPUs. The Maestro GUI was used as an interface to the software MacroModel 8.6 and 9.0 [6]. Molecular mechanics (MM) calculations (docking) and molecular dynamics (MD) simulations were performed using the AMBER* force field as implemented in MacroModel [6]. No cutoff was applied for the non-bonded interactions and the calculations were performed in the gas phase selecting the constant dielectric treatment (dielectric constant ε = 1.0). Restrained electrostatic potential (RESP) atomic partial charges [7], to be used in the docking and MD simulations, were obtained through the Amber molecular dynamics package [8], starting from electrostatic potential (ESP) derived charges, obtained from quantum

chemical calculations performed with the software Gaussian03 [9]. While already determined RESP charges were used for the protonated amido[4]resorcinarene $[\mathbf{M^S}{\cdot}H]^+$ (see Section 2.2) and for amphetamine **1** [1], new calculations were done for compounds **2** and **4** by performing the RESP fitting on the entire molecular structure. Newly calculated partial atomic charges are specified in the last column of the cartesian coordinate structures enclosed as Supporting Information (mol2 format).

Insights into the structure and the dynamics of the proton-bound $[\mathbf{M^S}{\cdot}H{\cdot}\mathbf{A}]^+$ adducts were obtained by recognition simulations, using two computational methodologies implemented in MacroModel, that is Monte Carlo Multiple Minimum (MCMM) statistical conformational search and constant temperature MD runs. In the case of the Monte Carlo approach, the conformational analysis of both interacting partners was coupled with random rototranslations (MOLS command) of the guest species relative to the $[\mathbf{M^S}{\cdot}H]^+$ host standing still in the 3D space (MCMM/MOLS docking).

A preliminary MCMM/MD study of the protonated host was done to analyze its flexibility. It consisted in 10,000 steps of Monte Carlo search performed on the four L-valinamido pendants at the lower rim (20 rotatable bonds) of each one of the two feasible cations, followed by MD simulations at 300 K on the lowest energy minima. In agreement with the results of this preliminary analysis on $[\mathbf{M^S}{\cdot}H]^+$, each MCMM/MOLS run on $[\mathbf{M^S}{\cdot}H{\cdot}\mathbf{A}]^+$ adduct was made of 5000 steps, in which the rotation of only eight rotatable bonds of $[\mathbf{M^S}{\cdot}H]^+$ (three at the chiral carbon atom of the protonated pendant, five in the pendant not involved in the network of hydrogen bonds at the lower rim) was added to the rotatable bonds of each guest. During the dockings a randomly variable number of rotatable bonds of each adduct, ranging from 2 to $N-1$ (N represents the overall number of variable torsion angles defined in the command file), was subjected to random step variations in the range 0–180°. With $[\mathbf{M^S}{\cdot}H{\cdot}\mathbf{1}]^+$, a total number of 11 torsional degrees of freedom was analyzed (the flexibility of the resorcinarene skeleton was not directly sampled) [1], with $[\mathbf{M^S}{\cdot}H{\cdot}\mathbf{3}]^+$ and $[\mathbf{M^S}{\cdot}H{\cdot}\mathbf{4}]^+$, this number increased to 12, while with $[\mathbf{M^S}{\cdot}H{\cdot}\mathbf{2}]^+$ the value of 13 rotatable bonds was reached. The rototranslations of the guest species were limited by the maximum values of 180° for the rotational angle and of 3 Å for the translational movement. Energy minimizations were performed using the Truncated Newton conjugate gradient (TNCG) procedure and were terminated when the energy gradient root mean square (rms) fell below 0.01 kJ mol^{-1} Å^{-1}. A comparison was performed among the heavy atoms of the output geometries to eliminate duplicate conformations, selecting 1.0 Å as the maximum allowable separation between couples of corresponding atoms after superimposition. All the unique conformers were saved that differed from the global minimum-energy conformation by less than 20 kJ mol^{-1}.

Constant temperature MD simulations with generation of the canonical ensemble were performed at 300 K with a standard time step of 1.0 fs. Such a time step did not require the use of SHAKE algorithm. Coupling between the temperature bath and the molecules was updated every 0.2 ps. The equilibration period was 50 ps for every run, while the total simulation times ranged from 10 to 20 ns. During each trajectory, a variable number of structures (frames) were sampled at regular intervals throughout the time course. Average MD structures were calculated by uniform weighting of the sampled frames. The frame closest to the average geometry, that is the so called "representative" structure, was selected and RMSD-compared with the lowest energy docking outputs to detect any divergence between the two approaches. Each recognition simulation (either docking and molecular dynamics) was performed two times starting from a different arbitrary input geometry to verify convergence (by result replication). When the application of such a procedure gave a different minimum, the corresponding recognition simulation was repeated until convergence to the global minimum. The convergence of the results guarantees the completeness of the study.

Molecular mechanics intermolecular energies (steric and electrostatic terms of the potential energy) between $[\mathbf{M^S}{\cdot}H]^+$ and the **A** guests were calculated by means of the MacroModel Component Interactions Pyton script, by application of the same force field parameters used in the other calculations.

3. Results and discussion

3.1. FT-ICR experiments

The proton-bonded $[\mathbf{M^S}{\cdot}H{\cdot}\mathbf{A}]^+$ ($\mathbf{A} = \mathbf{2^{R/S}}$, $\mathbf{3^{RS/SR}}$, and $\mathbf{4^{RR/SS}}$) adducts were generated by electrospray ionization (ESI) of suitable $\mathbf{M^S}/\mathbf{A}$ methanolic solutions in the source of the Fourier-Transform Ion Cyclotron Resonance Mass Spectrometer (FT-ICR) and then conveyed into the FT-ICR cell containing fixed concentrations of the pure enantiomers of 2-aminobutane, either $\mathbf{B^R}$ or $\mathbf{B^S}$. The selectivity of reaction (1) was checked by determining the rate of the **B**-to-**A** displacement in $[\mathbf{M^S}{\cdot}H{\cdot}\mathbf{A}]^+$ [10–18]. It was measured by monitoring the appearance of the relevant exchanged product, i.e., $[\mathbf{M^S}{\cdot}H{\cdot}\mathbf{B}]^+$, and the decay of the reactant $[\mathbf{M^S}{\cdot}H{\cdot}\mathbf{A}]^+$ as a function of time t. If I is the intensity of starting $[\mathbf{M^S}{\cdot}H{\cdot}\mathbf{A}]^+$ adduct at the delay time t and I_0 is the sum of the intensities of the starting adduct and of its exchanged products, mono-exponential $\ln(I/I_0)$ vs t plots were obtained for all the selected $[\mathbf{M^S}{\cdot}H{\cdot}\mathbf{A}]^+$ ($\mathbf{A} = \mathbf{2}$–$\mathbf{4}$) (corr. coeff. $0.997 < r^2 < 0.999$) (see, for instance, Figs. S1–S3 of Supporting Information). The good linearity of their decay curves confirms the view that the $[\mathbf{M^S}{\cdot}H{\cdot}\mathbf{A}]^+$ (A = **2**–**4**) adducts are thermally equilibrated before reacting with **B**. The pseudo-first-order rate coefficient k' of reaction (1) was obtained from the slopes of the relevant $\ln(I/I_0)$ vs t linear plots.

The second-order rate coefficients $k = k'/[\mathbf{B}]$ of Eq. (1) ($\mathbf{A} = \mathbf{2}$–$\mathbf{4}$) are listed in Table 1, together with those involving the diastereomeric $[\mathbf{M^S}{\cdot}H{\cdot}\mathbf{1^{R/S}}]^+$ adducts from the previous study [1]. Their values, compared with the relevant collision rate constant (k_C) [19], provide a measure of the percent efficiency of the reaction (eff = $100k/k_C$). In Table 1, the second-order rate coefficients k are denoted according to the configuration of the **A** and **B** molecules. When the chiral carbon nearest to the amino group of **A** has the same absolute configuration S of the chiral centers of the L-valinamido pendants of host $\mathbf{M^S}$, then the corresponding adduct is denoted as *homo* and the exchange second-order rate coefficients as k_{homo}. Obviously, when the chiral carbon nearest to the amino group of **A** has the opposite configuration R, then the corresponding adduct is denoted as *hetero* and the exchange second-order rate coefficients as k_{hetero}. Furthermore, in Table 1, the superscript R refers to the reaction with $\mathbf{B^R}$ (k^R) and the S to the reaction with $\mathbf{B^S}$ (k^S).

The kinetic effects of the $\mathbf{M^S}$ and **A** configuration are defined by the $\rho = k_{homo}/k_{hetero}$ ratios, while those of the **B** configuration by the $\zeta = k^R/k^S$ ones. A $\rho > 1$ value indicates that the **B**-to-**A** displacement 1 is faster with the *homo* adduct than with the *hetero* one. The opposite is true when $\rho < 1$. A $\rho = 1$ value corresponds to equal displacement rates. Analogously, a $\zeta > 1$ value indicates that the displacement of the **A** guest from a given adduct is faster with $\mathbf{B^R}$ than with $\mathbf{B^S}$. Again, the opposite is true when $\zeta < 1$. A $\zeta = 1$ value corresponds to equal displacement rates.

According to Table 1, the $[\mathbf{M^S}{\cdot}H{\cdot}\mathbf{2}]^+$ adducts exhibit a reaction selectivity ($\rho^R = 1.3 \pm 0.2$; $\rho^S = 1.4 \pm 0.1$) which is similar to that of $[\mathbf{M^S}{\cdot}H{\cdot}\mathbf{3}]^+$ ($\rho^R = \rho^S = 1.8 \pm 0.2$), but opposite to that of $[\mathbf{M^S}{\cdot}H{\cdot}\mathbf{1}]^+$ ($\rho^R = \rho^S = 0.4 \pm 0.1$). In contrast, the $[\mathbf{M^S}{\cdot}H{\cdot}\mathbf{4}]^+$ adducts are much less reactive (reaction efficiency: 0.2–0.3) and do not display any selectivity ($\rho^R = 0.9 \pm 0.2$; $\rho^S = 1.0 \pm 0.1$). These marked differences suggest that the presence and the location of the OH group on the

Table 1
Rate coefficients ($k \times 10^{-10}$ cm^3 molecule^{-1} s^{-1}) of the gas-phase reaction (1).

Adduct	Reaction enantioselectivities					Reaction efficiency[a]	
	$\mathbf{B^R}$ = R-(−)-$C_4H_9NH_2$		$\mathbf{B^S}$ = S-(+)-$C_4H_9NH_2$			$\mathbf{B = B^R}$	$\mathbf{B = B^S}$
	k^R	$\rho^R = k^R_{homo}/k^R_{hetero}$	k^S	$\rho^S = k^S_{homo}/k^S_{hetero}$	$\zeta = k^R/k^S$	$100k^R/k_C$	$100k^S/k_C$
$[\mathbf{M^S}\cdot H\cdot\mathbf{1^R}]^+_{hetero}$	1.03 ± 0.09	0.4 ± 0.1	0.83 ± 0.09	0.4 ± 0.1	1.2 ± 0.3	9	7
$[\mathbf{M^S}\cdot H\cdot\mathbf{1^S}]^+_{homo}$	0.40 ± 0.03		0.37 ± 0.03		1.1 ± 0.1	3	3
$[\mathbf{M^S}\cdot H\cdot\mathbf{2^R}]^+_{hetero}$	0.96 ± 0.06	1.3 ± 0.2	0.89 ± 0.06	1.4 ± 0.1	1.1 ± 0.1	8	8
$[\mathbf{M^S}\cdot H\cdot\mathbf{2^S}]^+_{homo}$	1.29 ± 0.09		1.27 ± 0.03		1.0 ± 0.1	11	11
$[\mathbf{M^S}\cdot H\cdot\mathbf{3^{SR}}]^+_{hetero}$	0.61 ± 0.03	1.8 ± 0.2	0.61 ± 0.06	1.8 ± 0.2	1.0 ± 0.1	5	5
$[\mathbf{M^S}\cdot H\cdot\mathbf{3^{RS}}]^+_{homo}$	1.13 ± 0.06		1.10 ± 0.03		1.0 ± 0.1	10	9
$[\mathbf{M^S}\cdot H\cdot\mathbf{4^{RR}}]^+_{hetero}$	0.033 ± 0.001	0.9 ± 0.2	0.028 ± 0.002	1.0 ± 0.1	1.1 ± 0.1	0.3	0.2
$[\mathbf{M^S}\cdot H\cdot\mathbf{4^{SS}}]^+_{homo}$	0.030 ± 0.001		0.029 ± 0.001		1.0 ± 0.2	0.2	0.2

[a] Reaction efficiency expressed by the percent ratio between the measured rate coefficients and the corresponding collision constant k_C, calculated using the trajectory calculation method (Ref. [19]).

side chain of the guest **A** play an important role in determining the structure and the relative stability of their diastereomeric adducts with $\mathbf{M^S}$. In general, the effect of the configuration of **B** on the reaction kinetics is not very pronounced ($1.0 \pm 0.1 < \zeta < 1.2 \pm 0.3$), thus corroborating previous computational evidence about the guest molecule as residing preferentially in a position external to the $\mathbf{M^S}$ cavity between two adjacent pendants (the *ext* position in Fig. 1) [1].

The different reaction efficiencies and selectivities of Table 1 raise the question as to whether they are due to kinetic factors, i.e., to differences in the relative stability of the transition structures involved in reaction (1), or to thermodynamic factors, i.e., to differences in the relative stability of the diastereomeric $[\mathbf{M^S}\cdot H\cdot\mathbf{A}]^+$ adducts. A detailed structural and energetic analysis of some representative $[\mathbf{M^S}\cdot H\cdot\mathbf{A}]^+$ aggregates is needed to answer this important question. This task has been undertaken by using molecular mechanics (MM) calculations and molecular dynamics (MD) simulations.

3.2. MM calculations and MD simulations on $[\mathbf{M^S}\cdot H]^+$

Because of its flattened-cone conformation of $[\mathbf{M^S}\cdot H]^+$, two sets of nonequivalent L-valinamido pendants can be discerned in the protonated host and denoted by white and green arrows in Fig. 3a. According to previous computational studies [20], the structure of the protonated host $[\mathbf{M^S}\cdot H]^+$ is rather rigid and is characterized by a network of intramolecular hydrogen bonds among three of the four L-valinamido pendants of the host, specifically among their amidocarbonyl centers. However, only one of the two sets of nonequivalent L-valinamido pendants of the host (the energetically most favored amidocarbonyls *p1* denoted by white arrows in Fig. 3a) was considered in that study. Although the structural and dynamic factors governing the enantioselectivity of $\mathbf{M^S}$ towards small guest species were fully elucidated [1], nevertheless no clear-cut correlation between the experimental enantioselectivity and the total potential energy of the simulated adducts could be obtained. This failure induced us to hypothesize that, in the $[\mathbf{M^S}\cdot H\cdot\mathbf{A}]^+$ adducts, the most favored protonation site may be other than that in $[\mathbf{M^S}\cdot H]^+$. This implies the need of modeling both possible boundary $[\mathbf{M^S}\cdot H]^+$ protomers, one with the proton at *p1* and the other at *p2* (denoted by green arrows in Fig. 3a).

The $[\mathbf{M^S}\cdot H]^+$ protomers with the proton at either of the two symmetrically nonequivalent sites *p1* or *p2* were investigated by two Monte Carlo searches on the four pendants followed by MD simulations at 300 K on low energy output structures. The results point to an intrinsic pre-organization of $[\mathbf{M^S}\cdot H]^+$ highlighted by its tendency to adopt a sort of rotatory folding involving three contiguous pendants (named hereafter as the "*amido network*", Fig. 3a–c).

In the case of protonation at *p1* (global minimum of the MCMM searches, named hereafter as the "*p1 cation*", colored in yellow in Fig. 3a) the *amido network* starts from the protonated pendant and extends counterclockwise over two H-bondings between adjacent amido groups. The 3D architecture is further rigidified by the orientation towards the center of the lower rim cavity of the estereal carbonyl of the *p2* valine belonging to the *amido network*. Finally, the protonated *p1* center binds the carbonyl ester of the *p2* valine not directly involved in the *amido network* by an additional H-bond.

In the lowest energy conformation of the "*p2 cation*" (colored in yellow in Fig. 3b), whose average energy content at 300 K is

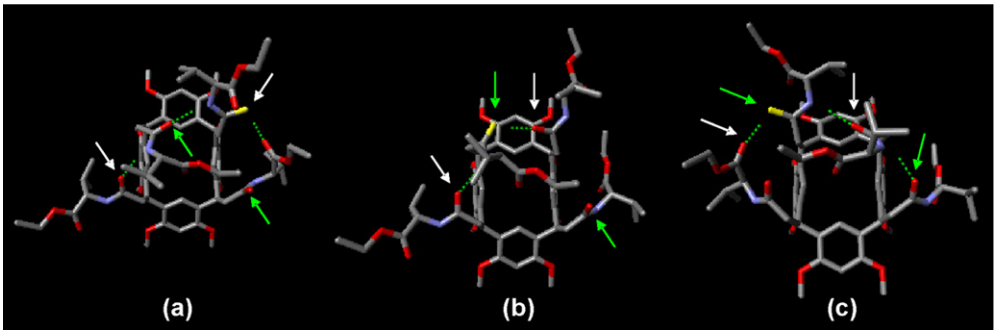

Fig. 3. The most favored protonation sites in 2,8,14,20-tetrakis(L-valinamido)resorcin[4]arene ethyl tetra-ester ($\mathbf{M^S}$) are its amidocarbonyls. Those located on symmetrically equivalent chiral pendants are indicated by arrows with the same color (white: *p1*; green: *p2*). The protonated amidocarbonyl in (a)–(c) is colored in yellow. (a) Global-minimum geometry of *p1*-protonated $\mathbf{M^S}$, the amido network (see text) starts from the yellow colored carbonyl and goes counterclockwise; (b) lowest energy geometry of *p2*-protonated $\mathbf{M^S}$; (c) 26 kJ mol^{-1} higher-energy geometry of *p2*-protonated $\mathbf{M^S}$, the amido network (see text) starts from the yellow colored carbonyl and goes clockwise. (For interpretation of the references to color in this figure caption, the reader is referred to the web version of the article.)

Table 2
Average host/guest potential energies calculated during MD simulations at 300 K.

Complex	Protonation at *p1* NBIE (kJ mol^{-1})	Protonation at *p2* NBIE (kJ mol^{-1})	Δ = (NBIE)$_{homo}$ − (NBIE)$_{hetero}$ (kJ mol^{-1})[a]	ρ
[**MS**·H·**1**$^{\mathbf{R}}$]$^+_{hetero}$	*−130*	−128	*−5*	0.4
[**MS**·H·**1**$^{\mathbf{S}}$]$^+_{homo}$	−130	*−135*		
[**MS**·H·**2**$^{\mathbf{R}}$]$^+_{hetero}$	−170	*−180*	*+10*	1.3–1.4
[**MS**·H·**2**$^{\mathbf{S}}$]$^+_{homo}$	−130	*−170*		
[**MS**·H·**3**$^{\mathbf{SR}}$]$^+_{hetero}$	−144	*−148*	*+8*	1.8
[**MS**·H·**3**$^{\mathbf{RS}}$]$^+_{homo}$	−134	*−140*		
[**MS**·H·**4**$^{\mathbf{RR}}$]$^+_{hetero}$	−137	*−166*	*−1*	0.9–1.0
[**MS**·H·**4**$^{\mathbf{SS}}$]$^+_{homo}$	*−167*	−132		

[a] NBIE: non-bonded intermolecular energy.

about 5 kJ mol^{-1} higher than that of the *p1* cation, the protonated pendant is the central one in the *amido network*. The H-bond distance between C–OH$^+$ at *p2* and O=C at *p1* is so short (1.64 Å) that a proton exchange among pendants cannot be excluded. Notably, a higher-energy *p2* cation geometry (about 26 kJ mol^{-1} above the lowest energy one) shows a counterclockwise *amido network* (protonated *p2* carbonyl colored in yellow in Fig. 3c), which features a mirror image disposition of pendants *p1* and *p2* with respect to the *p1* cation. The availability of the protonated carbonyl group for binding guests, always detected in our previous simulations and successfully verified *a posteriori* also in this study (see below), has suggested to consider this geometry for further dockings.

3.3. MM and MD calculations on diastereomeric [**M**$^{\mathbf{S}}$·H·**A**]$^+$ adducts

Assuming that the *amido network* in [**M**$^{\mathbf{S}}$·H]$^+$ can resist interaction with the **A** guest, the just described results allow to streamline MCMM/MOLS docking simulations on the [**M**$^{\mathbf{S}}$·H·**A**]$^+$ adducts by restricting explicit analysis of the host flexibility to the conformational search of pendants *p1* and *p2*. Any inconsistency with such a preliminary assumption would be revealed by the time evolution of the most stable [**M**$^{\mathbf{S}}$·H·**A**]$^+$ geometries during MD simulations. Moreover, the recent implementations in Macromodel of an algorithm allowing estimates of host/guest interaction energies [21] induced us to consider these quantities as a better descriptor of the kinetic enantioselectivity of the diastereomeric [**M**$^{\mathbf{S}}$·H·**A**]$^+$ adducts.

Once fixed our computational protocol, the clockwise *p1* and the counterclockwise *p2* geometries reported in Fig. 3a and c, respectively, have been used as an input for docking studies on the adducts of [**M**$^{\mathbf{S}}$·H]$^+$ with all the stereoisomers of neurotransmitters **A** = **1**–**4**. The lowest energy output structure of each adduct has been subsequently submitted to MD runs at 300 K.

Table 2 lists the average value of the force field based non-bonded intermolecular energy (NBIE) values (that is, the coulombic and Lennard–Jones terms between [**M**$^{\mathbf{S}}$·H]$^+$ and **A**) calculated along the frames of all the MD runs on the different [**M**$^{\mathbf{S}}$·H·**A**]$^+$ adducts. In most cases, the NBIE values are similar for either protonation states. This means that both states might be populated with some exceptions, including [**M**$^{\mathbf{S}}$·H·**2**$^{\mathbf{S}}$]$^+$, [**M**$^{\mathbf{S}}$·H·**4**$^{\mathbf{SS}}$]$^+$, and [**M**$^{\mathbf{S}}$·H·**4**$^{\mathbf{RR}}$]$^+$. Moreover, some relationship does exist between the difference Δ between the highest NBIE values of each adduct (reported in italic in Table 2 and referring to the most stable diastereomeric adducts) and the corresponding enantioselectivity ρ factors of Table 1. Thus, a positive Δ value always corresponds to $\rho > 1$ ([M^S·H·**3**$^{\mathbf{SR/RS}}$]$^+$ and [M^S·H·**2**$^{\mathbf{R/S}}$]$^+$), as expected if the kinetics of reaction (1) is essentially regulated by the magnitude of the interaction forces in the [**M**$^{\mathbf{S}}$·H·**A**]$^+$ adduct. Along the same line, the $\rho < 1$, measured with [**M**$^{\mathbf{S}}$·H·**1**$^{\mathbf{R/S}}$]$^+$, is fully accounted by its negative Δ value. Finally, the lack of diastereoselectivity exhibited by [**M**$^{\mathbf{S}}$·H·**4**$^{\mathbf{RR/SS}}$]$^+$ in reaction (1) ($\rho = 1$) is explained by their relatively small Δ value.

As illustrated in Table 1, although reactions of amine **B** with **3**$^{\mathbf{SR}}$ and **3**$^{\mathbf{RS}}$ are almost 20 times faster than those with **4**$^{\mathbf{SS}}$ and **4**$^{\mathbf{RR}}$, nonetheless they exhibit the highest enantioselectivity. This apparent discrepancy can be explained if the reactivity of the [**M**$^{\mathbf{S}}$·H·**A**]$^+$ adducts is related to the magnitude of the NBIE values, whereas their diastereoselectivity to the sign and the magnitude of the relevant Δ values. Both factors are strictly related to the intimate structural features of the adducts whose detailed description is reported in the Supporting Information (Figs. S4 and S5).

4. Conclusions

The experimental and computational results of the present work indicate that the stability and the reactivity of the adducts between ethanolamine neurotransmitters **A** = **2**–**4** and the chiral amido[4]resorcinarene receptor **M**$^{\mathbf{S}}$ depend on: (1) the relative position and the orientation of the hydroxyl and amino functionalities on the **A** side chain; (2) the presence of the methyl substituent on its N center; and (3) the specific amidocarbonyl center of **M**$^{\mathbf{S}}$ (whether *p1* or *p2*) proton-bonded to the amino group of **A**. These factors strongly influence the nature and the intensity of the noncovalent interactions in the [**M**$^{\mathbf{S}}$·H·**A**]$^+$ adducts and, therefore, their reactivity and selectivity. Accordingly, the poor reactivity and selectivity of the diastereomeric [**M**$^{\mathbf{S}}$·H·**4**$^{\mathbf{RR/SS}}$]$^+$ adducts is ascribed to the intense interactions between the pseudoephedrine enantiomers and the two symmetrically nonequivalent protonated sites *p1* or at *p2* of **M**$^{\mathbf{S}}$. Owing to their comparable magnitude, the diastereomeric [**M**$^{\mathbf{S}}$·H·**4**$^{\mathbf{RR/SS}}$]$^+$ adducts exhibit structures which are almost mirror images each other. In comparison, their [**M**$^{\mathbf{S}}$·H·**3**$^{\mathbf{SR/RS}}$]$^+$ analogues exhibit a greater reactivity and selectivity which are accounted for by the fact that the corresponding intracomplex interactions are significantly less intense and different in magnitude because of not so effective shape matching between the chiral side chain of ephedrine and the chiral pendants of **M**$^{\mathbf{S}}$.

Acknowledgements

Work supported by the Ministero dell'Istruzione dell'Università e della Ricerca (MIUR, COFIN), the Consiglio Nazionale delle Ricerche (CNR), and Istituto Pasteur Fondazione Cenci Bolognetti. B.B. gratefully acknowledges Project "FIRB 2003: RBNE034XSW_005" from MIUR (Ministero della Università e della Ricerca).

Appendix A. Supplementary data

Supplementary data associated with this article can be found, in the online version, at doi:10.1016/j.ijms.2010.01.017.

References

[1] B. Botta, A. Tafi, F. Caporuscio, M. Botta, L. Nevola, I. D'Acquarica, C. Fraschetti, M. Speranza, Chem. Eur. J. 14 (2008) 3585–3595.
[2] T.Z.E. Jones, D. Balsa, M. Unzeta, R.R. Ramsay, J. Neural Trasm. 114 (2007) 707–712, See also: R.V. Dunn, K.R. Marshall, A.W. Munro, N.S. Scrutton, FEBS J. 275 (2008) 3850–3858.
[3] See, for instance;
(a) R. Breslow, S. Bandyopadhyay, M. Levine, W. Zhou, ChemBioChem 7 (2006) 1491–1496;
(b) J.I. Gao, S. Ma, D.T. Major, K. Nam, J. Pu, D.G. Truhlar, Chem. Rev. (Washington, DC, United States) 106 (2006) 3188–3209;
(c) F. Hollfelder, A.J. Kirby, D.S. Tawfik, J. Org. Chem. 66 (2001) 5866–5874.
[4] B. Botta, G. Delle Monache, P. Salvatore, F. Gasparrini, C. Villani, M. Botta, F. Corelli, A. Tafi, E. Gacs-Baitz, A. Santini, C.F. Carvalho, D. Misiti, J. Org. Chem. 62 (1997) 932–938.
[5] D.A. Quagliato, P.M. Adae, E.M. Matelan, J. Org. Chem. 65 (2000) 5037–5042.
[6] F. Mohamadi, N.G.J. Richards, W.C. Guida, R. Liskamp, M. Lipton, C. Caufield, G. Chang, T. Hendrickson, W.C. Still, J. Comput. Chem. 11 (1990) 440–467, MacroModel, Schrödinger Inc.; Portland, OR 97204; http://www.schrodinger.com.
[7] C.I. Bayly, P. Cieplak, W.D. Cornell, P.A. Kollman, J. Phys. Chem. 97 (1993) 10269–10280.
[8] http://amber.scripps.edu/, University of California: San Francisco, CA (2004).
[9] www.gaussian.com Gaussian, Inc.: Pittsburgh, PA (2001).
[10] M. Speranza, F. Gasparrini, B. Botta, C. Villani, D. Subissati, C. Fraschetti, F. Subrizi, Chirality 21 (2009) 69–86.
[11] A. Tafi, B. Botta, M. Botta, G. Delle Monache, A. Filippi, M. Speranza, Chem. Eur. J. 10 (2004) 4126–4135.
[12] B. Botta, D. Subissati, A. Tafi, G. Delle Monache, A. Filippi, M. Speranza, Angew. Chem. Int. Ed. 43 (2004) 4767–4770.
[13] A. Filippi, F. Gasparrini, M. Pierini, M. Speranza, C. Villani, J. Am. Chem. Soc. 127 (2005) 11912–11913.
[14] B. Botta, F. Caporuscio, I. D'Acquarica, G. Delle Monache, D. Subissati, A. Tafi, M. Botta, A. Filippi, M. Speranza, Chem. Eur. J. 12 (2006) 8096–8105.
[15] B. Botta, F. Caporuscio, D. Subissati, A. Tafi, M. Botta, A. Filippi, M. Speranza, Angew. Chem. Int. Ed. 45 (2006) 2717–2720.
[16] F. Gasparrini, M. Pierini, C. Villani, A. Filippi, M. Speranza, J. Am. Chem. Soc. 130 (2008) 522–534.
[17] B. Botta, C. Fraschetti, F.R. Novara, A. Tafi, F. Sacco, L. Mannina, A.P. Sobolev, J. Mattay, M.C. Letzel, M. Speranza, Org. Biomol. Chem. 7 (2009) 1798–1806.
[18] C. Fraschetti, M. Pierini, C. Villani, F. Gasparrini, S. Levi Mortera, M. Speranza, Chem. Commun. (2009) 5430–5432.
[19] T. Su, J. Phys. Chem. 88 (1988) 4102–4103;
T. Su, J. Phys. Chem. 89 (1988) 5355–5356.
[20] B. Botta, M. Botta, A. Filippi, A. Tafi, G. Delle Monache, M. Speranza, J. Am. Chem. Soc. 124 (2002) 7658–7659.
[21] http://www.schrodinger.com/Download.php?mID=8&sID=50&cID=10004#Molecular_Mechanics; script name: component interactions.py.